INTERNATIONAL JOURNAL FOR NUMERICAL METHODS IN FLUIDS, VOL. 5, 577–592 (1985)

AN INVISCID MODEL OF UNSTEADY AEROFOIL FLOW WITH FIXED UPPER SURFACE SEPARATION

M. VEZZA AND R. A. McD. GALBRAITH

Department of Aeronautics and Fluid Mechanics, University of Glasgow, Glasgow G12 8QQ, U.K.

SUMMARY

Presented in this paper is a new method for the prediction of unsteady, incompressible separated flow over a two-dimensional aerofoil. The algorithm was developed from an existing unsteady potential flow model[1] and makes use of an inviscid formulation for the flow field. The aerofoil is represented by vortex panels of linearly varying strength which are piecewise continuous at the corners. Discrete vortices with finite cores are used to model the separating shear layers.

Following a brief summary of unsteady separation modelling, the theoretical framework is presented and the subsequent numerical implementation is discussed in detail.

Results are given for flows which tend asymptotically to the steady state and conclusions are drawn regarding the usefulness of the method.

KEY WORDS Unsteady Separation Discrete Vortex Aerofoil Wake Inviscid

INTRODUCTION

The study of phenomena associated with unsteady flow around aerofoils has been of consuming interest to aerodynamicists for many years. An understanding of such flows is important, for instance, in the design of helicopter rotors. In this case during forward flight transonic effects are important for the half cycle of advancing blade motion, and dynamic stall is a predominant feature while the blade is retreating. The progress which has been made,[2] both experimentally and computationally, in these areas is also of benefit to those considering the performance of turbomachinery and wind turbines etc.

The discrete vortex method has been applied to unsteady aerofoil problems for some time. Geising,[3] Basu and Hancock[4] and the present authors[1] have used the method to predict unsteady, incompressible inviscid flows, whereas Ham,[5] Baudu *et al.*[6] and Ono *et al.*[7] have had some success in modelling unsteady, incompressible, separated flows, Clements and Maull[8] provided an early history of the method, and made subsequent use of it to model vortex shedding from a square based body. Other more recent uses of the method have been the asymptotically steady analyses of Sarpkaya[9] and Katz,[10] who considered a flat plate and a thin cambered aerofoil, respectively. These latter efforts highlight the attempts that have been made to reproduce what are essentially viscous phenomena by the use of inviscid algorithms. All these incorporate the assumption that the flow is irrotational over the entire region except at the body and its wake elements. In such schemes, the vorticity shed from the body is usually derived from velocities sampled at the edges of the shear layer, an approach validated by the experiments of Fage and Johansen[11] and by the analysis of boundary layer separation on aerofoils by Sears.[12,13]

0271–2091/85/060577–16$01.60

Received February 1985

Recently the detailed mathematical and numerical techniques associated with discrete vortex methods were reviewed by Leonard.[14] Application of the point vortex, vortex blob and newer contour dynamics methods to two-dimensional vortical flows were discussed as well as developments in three-dimensional vortex methods. Leonard was subsequently part of a team which incorporated the vortex blob, or core, method into a new numerical scheme for the prediction of separated flows.[15]

Three versions of the original algorithm were developed; a pure vortex method, a method with added quasi-steady integral boundary layer calculations, and a method which incorporated a truly unsteady implicit finite difference boundary layer scheme. Some valuable and interesting results were presented for a range of bluff body, aerofoil and tilt rotor problems. Further development is, however, needed, especially to improve on the drag predictions.

Presented in this paper are the first results from a new method to predict the unsteady flow over an aerofoil undergoing upper surface separation. The method is of the inviscid type and uses vortices with finite cores. Reliance is not placed on the explicit evaluation of the shear velocities for the determination of the shed vorticity, which is, rather, one of the variables in a 'Kutta' condition. The method was developed from an existing unsteady potential flow model,[1] and the location of the separation point is a necessary input into the algorithm.

THEORETICAL DESCRIPTION OF MODEL

The model at time t_m, is set up as shown in Figure 1. The aerofoil is represented by N panels from upper to lower trailing-edge over which there is placed a vortex sheet of linearly varying strength that is piecewise continuous at the panel corner points. With upper surface separation present, the distribution of vorticity within the separated zone is constrained to take starting and finishing values of zero. The circulation around the aerofoil is Γ_m, where $\Gamma_m = \int \gamma ds$, and the vorticity shed at previous times is represented by discrete vortices except in the region close to the upper surface separation point, where it takes the form of $N_p - 1$ constant strength vortex panels. Two additional constant strength vortex panels appear at time t_m, one at each separation

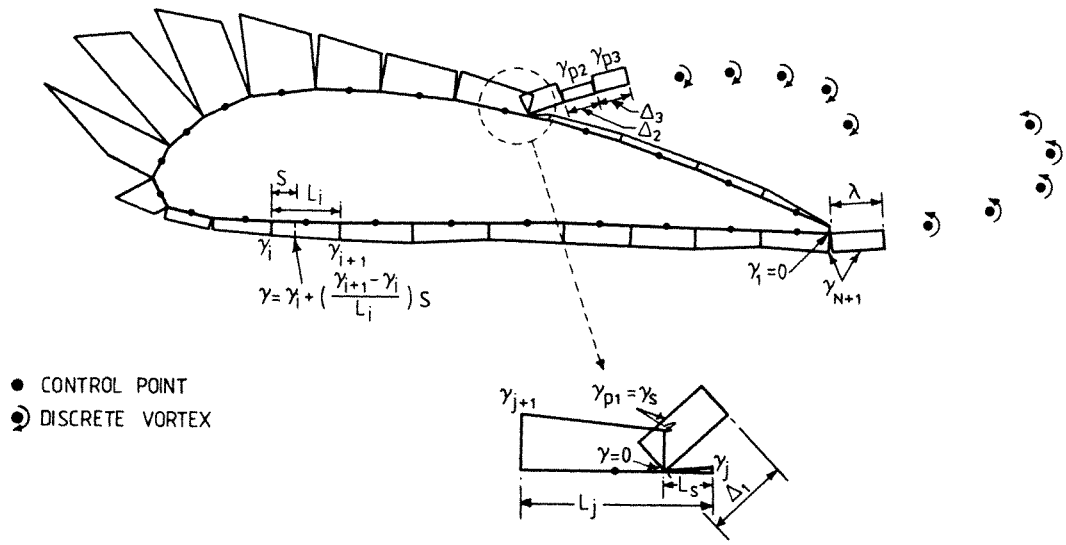

Figure 1. Unsteady separation model at time t_m

point, to account for the latest change in aerofoil circulation, in accordance with Kelvin's theorem.[16] The strengths of the emanating sheets are determined by making use of Helmoltz's theorem[17] of continuity of vorticity which, when applied with the former theorem, results in the following condition:

$$\Delta_1 \gamma_s + \lambda \gamma_{N+1} = \Gamma_{m-1} - \Gamma_m, \tag{1}$$

where Δ_1 and λ are the lengths of the respective panels.

In order to obtain a solution for the unknown bound vortex sheet strengths, the boundary condition of zero flow normal to the surface is applied at the mid-points (control points) of the aerofoil panels resulting in the following system of equations.

$$\mathbf{U}\cdot\hat{\mathbf{n}}_i + \sum_{j=2}^{N} A_{ij}\gamma_j + A_{i1}\gamma_s + A_{iN+1}\gamma_{N+1} + \sum_{g=2}^{N_p} A_{ig}\gamma_{pg} + \sum_{g=1}^{N_v} G_{ig}K_g = 0, \qquad i = 1, 2, \ldots, N. \tag{2}$$

The second, third and fourth terms in equation (2) are the normal induced velocities at the ith control point due to the bound vortex sheet and the two separating panels at time t_m, respectively. These terms contain the unknown vortex strengths, whereas the first, fifth and sixth terms can be completely evaluated and are the normal induced velocities at the ith control point due to the free stream, the remaining wake panels and all wake vortices, respectively. The theoretical details associated with equations (1) and (2) are considered in Reference 18.

The expressions (1) and (2) amount to a system of $N + 1$ simultaneous equations that are linear in the $N + 1$ unknown γ values. However, as Δ_1 and λ are also unknown a solution can be obtained only by iteration from initial values assigned to both of these variables. It follows that the iterative scheme must incorporate some means of assigning new values to Δ_1 and λ and this is achieved by considering the Bernoulli equation as it applies to vortex sheets.

The dynamical boundary conditions for vortex sheets have been examined by Geising[19] and a similar approach is used here. If we assume that a separated wake, as illustrated in Figure 2, gives rise to two isolated regions R_1 and R_2 with total heads h_1 and h_2, respectively, then the Bernoulli equation applied across each separation point yields the following results (see Figure 2);

Upper surface separation point

$$\left(\frac{p_a}{\rho} + \frac{\gamma_a^2}{2} + \frac{\partial \phi_a}{\partial t}\right) - \left(\frac{p_{a'}}{\rho} + \frac{\gamma_{a'}^2}{2} + \frac{\partial \phi_{a'}}{\partial t}\right) = h_1 - h_2 = \Delta h$$

$$\Rightarrow \quad \frac{\gamma_a^2}{2} = \frac{\partial}{\partial t}(\phi_{a'} - \phi_a) + \Delta h = \frac{\partial}{\partial t}(\Delta \phi_a) + \Delta h, \quad \text{with } p_a = p_{a'}$$

$$\Rightarrow \quad \frac{\gamma_s^2}{2} = \frac{\partial}{\partial t}\Delta \phi_s + \Delta h. \tag{3}$$

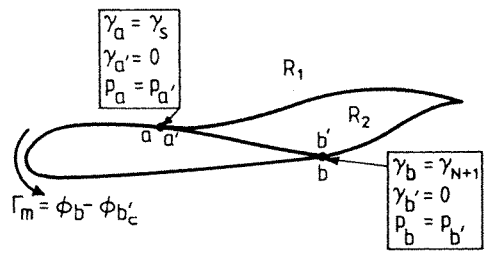

Figure 2. Inviscid formulation

Trailing-edge separation point

$$\left(\frac{p_b}{\rho}+\frac{\gamma_b^2}{2}+\frac{\partial\phi_b}{\partial t}\right)-\left(\frac{p_{b'}}{\rho}+\frac{\gamma_{b'}^2}{2}+\frac{\partial\phi_{b'}}{\partial t}\right)=h_1-h_2=\Delta h$$

$$\Rightarrow \quad \frac{\gamma_b^2}{2}=\frac{\partial}{\partial t}(\phi_{b'}-\phi_b)+\Delta h=\frac{\partial}{\partial t}(\Delta\phi_b)+\Delta h, \quad \text{with } p_b=p_{b'}$$

$$\Rightarrow \quad \frac{\gamma_{N+1}^2}{2}=\frac{\partial}{\partial t}(\Delta\phi_{N+1})+\Delta h. \tag{4}$$

Substracting (4) from (3) we get

$$\frac{\gamma_s^2}{2}-\frac{\gamma_{N+1}^2}{2}=\frac{\partial}{\partial t}(\Delta\phi_s-\Delta\phi_{N+1}). \tag{5}$$

In order to simplify the right hand side of equation (5) we acknowledge that

$$\phi_{a'}-\phi_{b'}+\phi_a-\phi_{a'}+\phi_b-\phi_a+\phi_{b'}-\phi_b=0$$

$$\Rightarrow \quad \phi_{a'}-\phi_{b'}+\phi_b-\phi_a=\Delta\phi_s-\Delta\phi_{N+1}.$$

The left hand side represents the circulation around the aerofoil, Γ_m, and therefore

$$\frac{\gamma_s^2}{2}-\frac{\gamma_{N+1}^2}{2}=\frac{\partial\Gamma_m}{\partial t}\simeq\frac{\Gamma_m-\Gamma_{m-1}}{\Delta t} \tag{6}$$

Equation (6), which is the unsteady 'Kutta' condition, can be derived by considering the boundary layer, which in this case is infinitely thin, at the separation points as was shown by Sears.[12,13] This is an example of the link between the viscous nature and inviscid dynamics of separation as the boundary layer thickness diminishes.

By examining equations (1), (3), (4) and (6) it will become apparent that the relevant iterative scheme for Δ_1 and λ is

$$\Delta_1=\left|\frac{\gamma_s}{2}\right|\Delta t,$$

$$\lambda=\left|\frac{\gamma_{N+1}}{2}\right|\Delta t.$$

Within the iterative cycle, the trailing edge panel is aligned with the local stream direction but, for numerical reasons which will be discussed later, this is not the case for the upper surface panels.

Once a converged solution has been obtained, the unsteady pressure coefficient is determined from Bernoulli's equation. In region R_1 (see Figure 2) this is

$$C_p=1-\frac{\gamma^2}{U^2}-\frac{2}{U^2}\frac{\partial\phi}{\partial t}.$$

In region R_2 the equation becomes

$$\begin{aligned}C_p&=1-\frac{\gamma^2}{U^2}-\frac{2}{U^2}\frac{\partial\phi}{\partial t}-\frac{2}{U^2}\Delta h\\&=1-\frac{\gamma^2}{U^2}-\frac{2}{U^2}\left[\frac{\partial\phi_a}{\partial t}+\frac{\partial\Delta\phi_a}{\partial t}+\frac{\partial}{\partial t}(\phi-\phi_{a'})+\Delta h\right]\\&=1-\frac{\gamma^2}{U^2}-\frac{2}{U^2}\frac{\partial\phi_c}{\partial t}-\frac{\gamma_s^2}{U^2},\end{aligned}$$

i.e.

$$C_p = 1 - \frac{(\gamma^2 + \gamma_s^2)}{U^2} - \frac{2}{U^2}\frac{\partial \phi_c}{\partial t},$$

where ϕ_c = continuous potential in region R_2.

The potential function is approximated by integrating the velocity field from upstream of the aerofoil to the leading edge and then around the surface, proceeding through the upper surface separation point in a continuous manner. The term $\partial\phi/\partial t$ is taken as $(\phi_m - \phi_{m-1})/\Delta t$, and the loads are determined by integrating the pressure distribution.

Once a complete solution has been obtained at time t_m, the model is then set up for time t_{m+1}. Existing vortices are convected to their new positions by calculating the velocities of their centres and using the first order Euler scheme:

$$\mathbf{r}_{vm+1} = \mathbf{r}_{vm} + \mathbf{q}_{vm}(t_{m+1} - t_m).$$

The same scheme as above is used to convect the extra trailing-edge panel to its new position as a discrete vortex. The upper surface panels, however, are treated differently, as detailed in the next section.

COMPUTATIONAL DETAILS

Upper surface separation

As illustrated in Figure 1 the separation point is located on one of the aerofoil panels between two corner points, as this positioning is essential if a solution is to be obtained. Restrictions which follow from this are:

(i) The separation point must be kept away from the corner points, otherwise there is one less unknown and a solution cannot be obtained.
(ii) The separation point must be kept away from the control points, otherwise infinite velocity components arise and the solution is meaningless.

Considering (i) and (ii), the best location for the separation point would be either at a distance of one quarter or three quarters of the panel length from one of the corner points; however numerical experiments have shown that the latter of these positions yields the most stable results. If separation occurs on the first panel a fully attached potential flow solution is obtained via an existing model.[1]

At the end of each time step the vorticity emanating from the upper surface does not immediately take the form of a discrete vortex but remains as a sheet for a number of time steps. The reason for this is illustrated in Figure 3, where the velocity components of a constant strength vortex panel and an equivalent point vortex, placed at the centre of the panel are plotted at various stations. From this Figure it may be seen that the discrete vortex approximation to a vortex sheet is very poor close to the sheet which leads, in this case, to an erroneous solution in the wake immediately downstream of the separation point. In arriving at a method of convecting this vorticity various schemes were tried:

(i) The velocity, $\bar{q}$, at each of the panel ends (taken as the mean of the control point velocities on either side) was calculated and hence the new length, $\Delta_{new} = \bar{q}\Delta t$ was computed. The vorticity was adjusted to maintain the overall panel circulation, i.e.

$$\gamma_{new} = \frac{(\gamma\Delta)_{old}}{\Delta_{new}}.$$

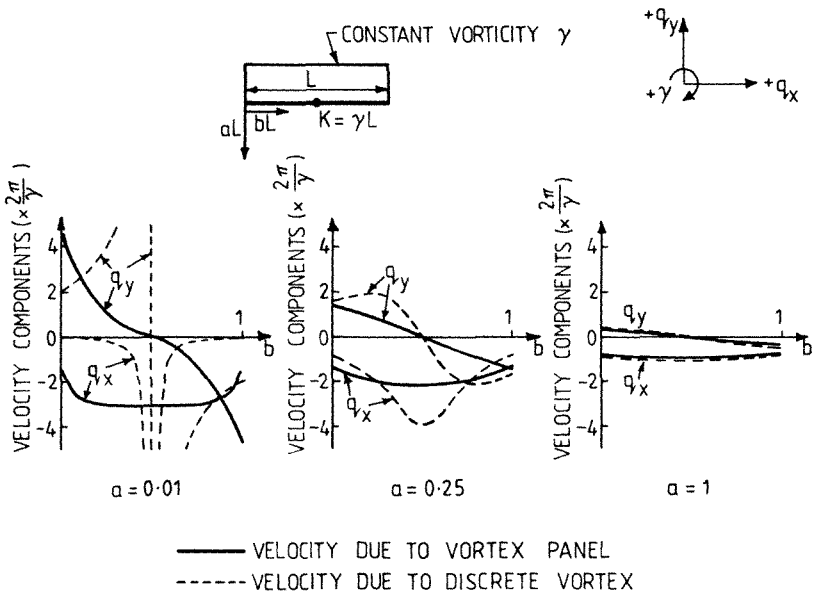

Figure 3. Comparison between the local velocity fields induced by a vortex panel and an equivalent discrete vortex

(ii) Panels were adjusted so that the vorticity strengths were the same as that at the separation point, i.e. $\gamma_{p2} = \gamma_{p3} = \gamma_{p4} = \cdots = \gamma_s$ The length were then computed from

$$\Delta_{new} = \frac{(\gamma_s \Delta)_{old}}{\gamma_{snew}}.$$

(iii) Panels were convected as a whole, i.e. $\Delta_{new} = \Delta_{old}$, $\gamma_{new} = \gamma_{old}$.

Scheme (i) proved to be too unstable when the velocity field around the separation point became erratic, leading to massive fluctuations in length and vorticity. Scheme (ii) suffered from similar stability problems due to the fact that large fluctuations in γ_s were propagated immediately throughout the near wake. Greatest stability was achieved with scheme (iii) and this is due to the fact that any fluctuations in γ_s only propagate one panel at a time, thereby avoiding massive instantaneous changes in the local velocity field.

Unlike the trailing-edge panel, geometric restrictions have been introduced to control the separated upper surface panels. The angle between the first panel and the local surface tangent, θ_p, is fixed and the angular deflection of each subsequent panel has an upper limit of $\Delta\theta_p$.

Once the panels have been convected as described above, the outermost panel becomes a discrete vortex, except at the start when the wake contains fewer than N_p panels.

Discrete vortex modelling

Initially point vortices were used to represent the shear layers. However, it was soon realized that stable solutions would not be obtained, owing to the singular nature of the flow in the vicinity of such vortices along with their proximity to the aerofoil surface. To overcome this problem, and obtain acceptable solutions, vortices with finite cores have been used. The resulting vorticity field can be written as follows:

$$\omega(\mathbf{r}) = \frac{1}{2\pi} \sum_{g=1}^{N_v} K_g \gamma_v(|\mathbf{r} - \mathbf{r}_g|), \tag{7}$$

where the function γ_v describes the distribution of vorticity within the core and satisfies the normalizing condition, $\int_0^\infty \gamma_v r dr = 1$. The velocity field is obtained by inserting equation (7) into the Biot–Savart equation to obtain[15]

$$\mathbf{q} = \frac{1}{2\pi} \sum_{g=1}^{N_v} K_g \eta(|\mathbf{r} - \mathbf{r}_g|) \begin{pmatrix} y_g - y \\ x - x_g \end{pmatrix},$$

where η is a function which makes the velocity regular throughout the core and is defined by the equation

$$\frac{d}{dr}(r^2\eta) = r\gamma_v.$$

Three types of core have been used (σ is the core radius):

(i) $\gamma_v = \dfrac{1}{\sigma r}$, $\mathbf{q} = \dfrac{1}{2\pi} \sum_{g=1}^{N_v} \dfrac{K_g \hat{\mathbf{t}}_n}{\sigma}$, inside core, i.e. constant velocity.

(ii) $\gamma_v = \dfrac{2}{\sigma^2} e^{-(r^2/\sigma^2)}$, $\mathbf{q} = \dfrac{1}{2\pi} \sum_{g=1}^{N_v} \dfrac{K_g}{r}(1 - e^{-(r^2/\sigma^2)})\hat{\mathbf{t}}_n$, throughout flow field.

(iii) $\gamma_v = \dfrac{2}{\sigma^2}$, $\mathbf{q} = \dfrac{1}{2\pi} \sum_{g=1}^{N_v} \dfrac{K_g}{\sigma^2} \mathbf{r}_n$, inside core, i.e. constant vorticity.

All of the results presented herein have been obtained using core (iii).

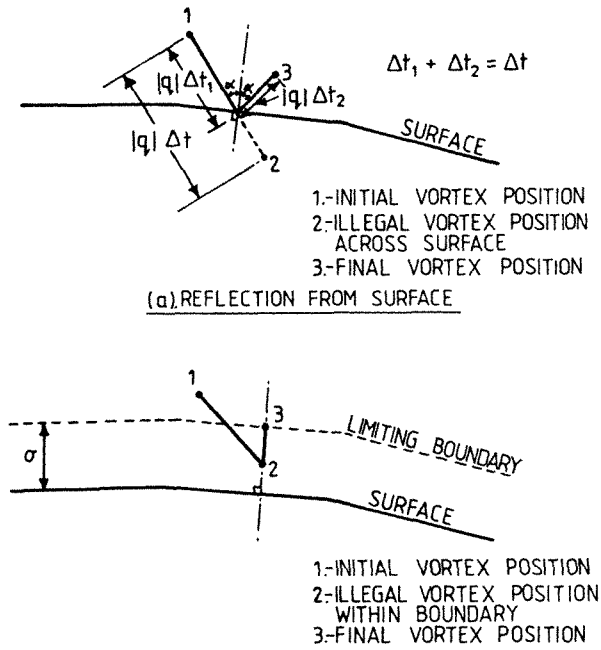

Figure 4. Restrictions on vortex motion

Once the vortices have been released into the stream they convect according to the induced velocities at their centres. It has been found necessary, however, to impose restrictions whenever unacceptable motions occur. These motions are due to an inappropriate time step for vortices close to the surface of the aerofoil. If left unhindered these may cross over the aerofoil surface. Initially such vortices were eliminated from the computation, but this produced unacceptable peaks in circulation and lift and so a different scheme was developed whereby they were reflected from the surface. This was an improvement but did not stop the problem of some vortices settling very near to the surface, and hence not convecting downstream.

This problem has been resolved by further ensuring that all vortices are kept outwith a given distance from the surface. At present this distance has been taken to be equal to the core radius, σ, and any vortex found within this region is relocated at the limiting boundary along the normal to the surface. Vortices that are close to the separation point very often do not reach this boundary for a few time steps and in such cases the temporary limiting distance used is the maximum normal distance to the surface yet achieved. Figure 4 illustrates these restrictions.

The large amount of time expended when vortex methods are used in computations usually dictates that a limit be placed on the total number of vortices contained in the wake. This is achieved by suitable coalescence. Vortices may be coalesced for other computational reasons, such as the prevention of wake disruption[9] caused by vortices of opposite sign. In the model described herein, two methods of coalescing vortices were used, one for each of two regions:

(i) Within a distance, D_0, of the aerofoil surface, vortices of opposite sign which come closer than a certain distance, D_v, are coalesced into a single equivalent vortex. The total circulation is conserved but not the first moment of vorticity as this would result in the combined vortex being far removed from the immediate vicinity. Instead, the location is calculated as if both vortices were of the same sign, i.e. $z_3 = (|K_1|z_1 + |K_2|z_2)/(|K_1| + |K_2|)$ where z_3 is the new position and z_1 and z_2 are the respective positions of the two vortices.

(ii) Outwith a distance, D_0, of the aerofoil surface any two vortices are coalesced if an error criterion is satisfied. The total circulation and the first moment of vorticity are conserved in the combination, which is carried out only if the error is less than a certain value, e_v. The expression used to calculate this error is similar to that used in Reference 15:

$$\left|\frac{K_1 K_2}{K_1 + K_2}\right| \frac{|z_1 - z_2|^2}{\Delta t d_1^{1\cdot5} d_2^{1\cdot5}} < e_v$$

The two methods are needed for the following reasons: in the region close to the aerofoil it is desirable to coalesce vortices of opposite sign, and this would not be a likely result of implementing method (ii) due to the error criterion; in this same region it is undesirable that vortices of the same sign be coalesced as this leads to stronger vortices and hence larger velocity gradients on the surface which can produce unstable results; in the region far from the surface the method should automatically coalesce vortices which are further apart than those in the close-in region, and method (ii) does this. It should be noted that the most recent N_c vortices to be shed are not involved in coalescence, so that the shear layer can initially remain relatively undisturbed.

Miscellaneous points

All of the results presented in the next section were obtained using a thirty panel representation of the aerofoil, as this number has been found to be satisfactory.[1] To calculate the velocity potential, a reference point is located three chord lengths upstream from the leading-edge and the change in potential calculated across each of thirty equal length panels which form a line

between both points. The choice of time step was a balance between the cost of the computation, the flow resolution required and the sensitivity of the solution to the length $\Delta_1 \propto \Delta t$. For all cases here, $\Delta t U/c = 0{\cdot}05$.

Four iterations are carried out per time step, as this number was found to be sufficient for acceptable convergence. The numerical parameters that were assigned the same value in all of the tests were $N_p = 4$, $N_c = 20$, $\theta_p = 10°$, $\sigma = 0{\cdot}05$, $D_0 = 1$, $D_v = 0{\cdot}1$, $e_v = 5 \times 10^{-4}$. Others are mentioned in the next section.

RESULTS

Figure 5 illustrates the results obtained following a step change in incidence from 0–18·25° for the NASA GA(W)-1 aerofoil. For this test $\Delta\theta_p = 0°$ and $x_s/c = 0{\cdot}575$. From Figure 5(a) it may be seen that the wake at $tU/c = 15$ consists of two well-defined shear layers which come together a short distance downstream followed by a thin region which extends far downstream while gradually opening out. This representation compares well with other wake models,[20,21] and there is no need to make initial assumptions concerning the wake shape. Figures 5(b) and 5(c) show the time dependent behaviour of the normal force and quarter chord moment. Although the initial response will not be physically accurate as the fixed separation point does not correctly model the true initial conditions, the approach to a steady value can be observed. The build-up in pressure near the leading-edge to the steady state is particularly evident in Figure 5(d) and the settled chordwise pressure distribution shown in Figure 5(e), compares very favourably with the experimental data[22] ($Re = 6{\cdot}3 \times 10^6$, $M = 0{\cdot}15$). An isometric projection of the pressure–time history is presented in Figure 5(f) and illustrates well he constant pressure region downstream of the separation point.

A step change from 0–20·05° was applied to the same aerofoil and Figure 6 illustrates the results obtained with $\Delta\theta_p = 0°$ and $x_s/c = 0{\cdot}475$. The shear layers in Figure 6(a) enclose a larger near wake region than that which was formed in the previous case although the thin far wake is similar. The normal force and quarter chord moment approach a steady value in Figures 6(b) and 6(c), and the build up in leading-edge pressure in Figure 6(d) is more marked than that in Figure 5(d). The good agreement of the settled solution with the measurements is evident in Figure 6(e).

Figure 6(f) illustrates the pressure–time history and provides a good view of the build-up to the steady state as well as the constant pressure region.

Figure 7 illustrates results obtained from a test where separation occurs near to the leading-edge after a step change in incidence from 0–21·14°, again using the same aerofoil. In this case $\Delta\theta_p = 3°$ and $x_s/c = 0{\cdot}125$. From Figure 7(a) it can be seen that the shear layer emanating from the upper surface starts to break up soon after it is shed and this is due to the more severe flow-field perturbations which accompany increasing amounts of separation. The result of this is that the near wake is wide and the far wake is no longer thin, exhibiting a periodic structure composed of alternately signed vortex clusters. The initial response of the normal force and quarter chord moment in Figures 7(b) and 7(c) corresponds to the passage of the first vortex cluster, although the forward movement of the separation point has not been modelled. The moment exhibits more of the oscillatory nature of the flow whereas the normal force is not unduly perturbed in its approach to a steady value. Owing to massive upper surface separation the behaviour of the leading-edge pressure, illustrated in Figure 7(d), is markedly different from the previous cases, and the computed pressure distribution compares very favourably, Figure 7(e), with the measured data. The wake pressure is not always constant, owing to the passage of vortices over the aerofoil; however, for comparison purposes a computed pressure distribution has been chosen, near

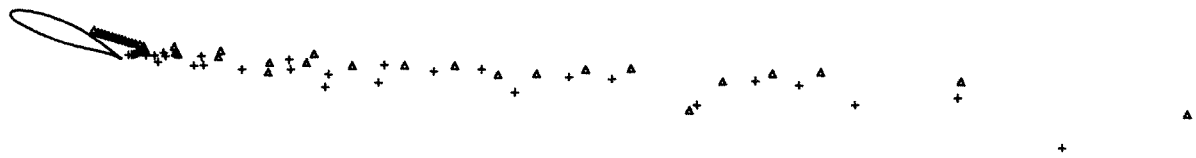

(a) Wake at $tU/c = 15$
△ clockwise circulation + anticlockwise circulation

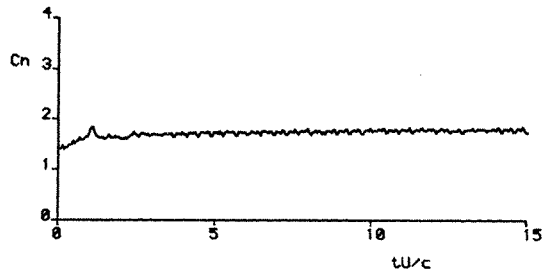

(b) Cn vs tU/c

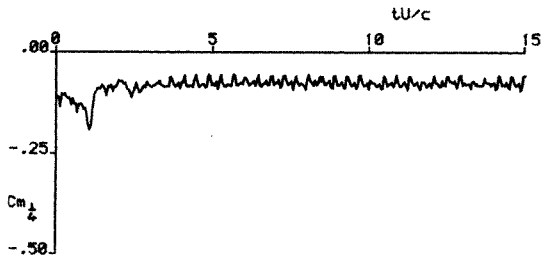

(c) $Cm_{\frac{1}{4}}$ vs tU/c

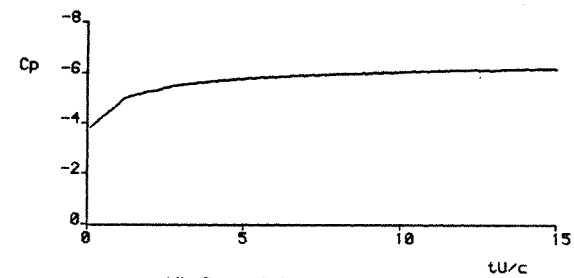

(d) Cp vs tU/c at $x/c = 0.025$

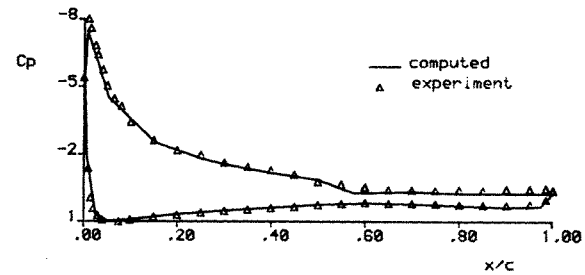

(e) Comparison between computed and steady experimental Cp

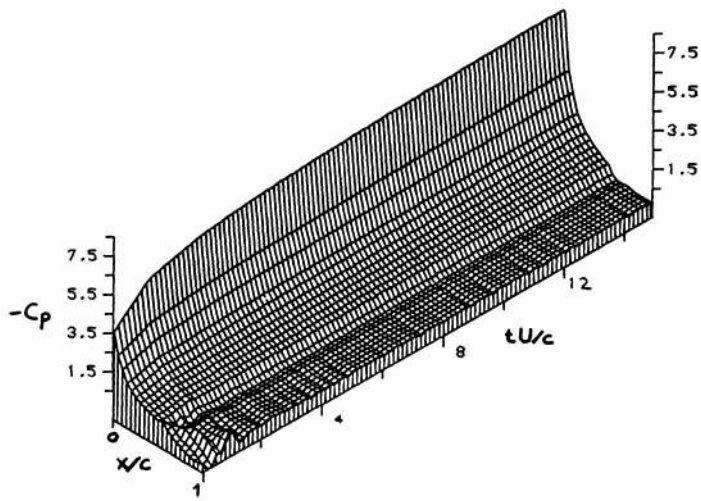

(f) Pressure–time history

Figure 5. Results obtained following a step change in incidence from $0 \rightarrow 18{\cdot}25°$ using the GA(W)-1 aerofoil

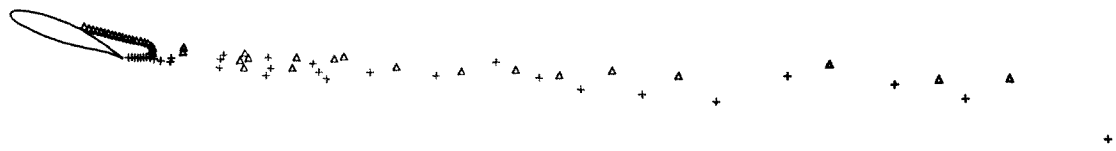

(a) Wake at tU/c = 15
△ clockwise circulation + anticlockwise condition

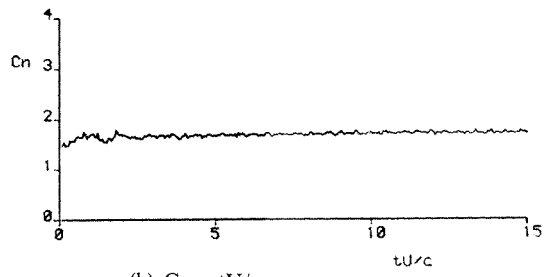

(b) Cn vs tU/c

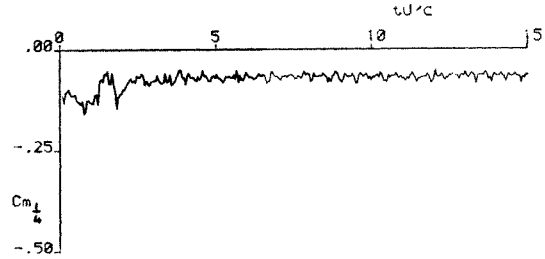

(c) $Cm_{\frac{1}{4}}$ vs tU/c

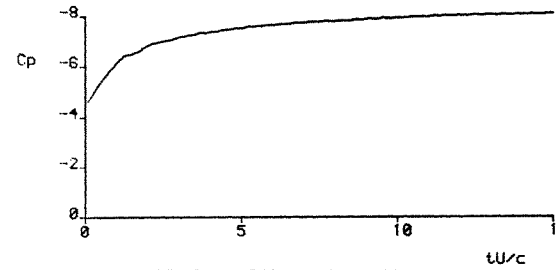

(d) Cp vs tU/c at x/c = 0·025

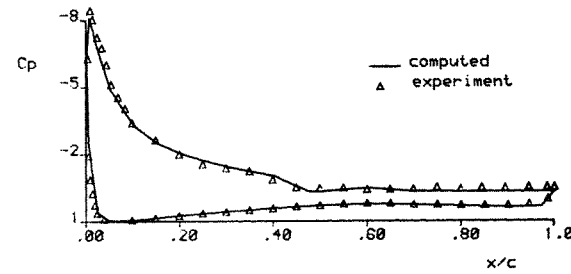

(e) Comparison between computed and steady experimental Cp

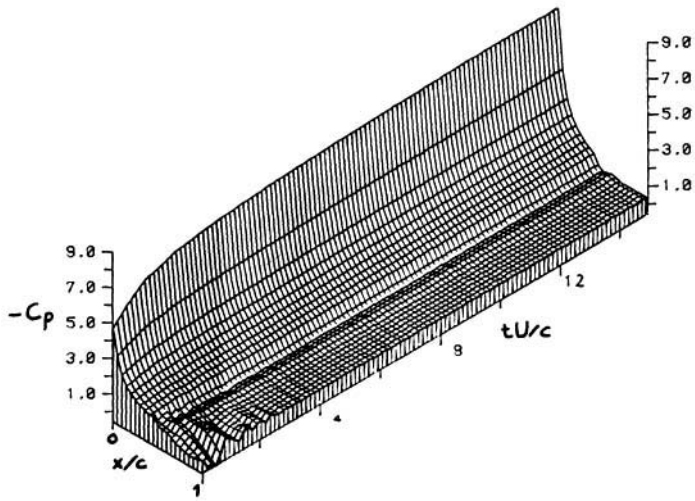

(f) Pressure–time history

Figure 6. Results obtained following a step change in incidence from 0 → 20·05° using the GA(W)-1 aerofoil

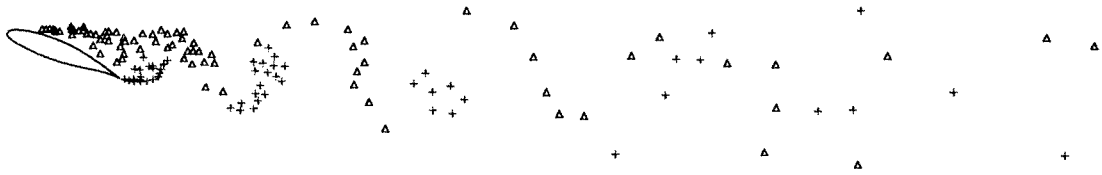

(a) Wake at tU/c = 20
△ clockwise circulation + anticlockwise circulation

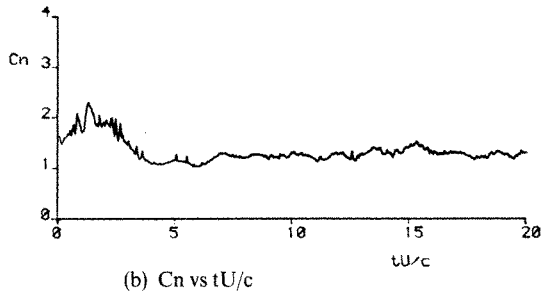

(b) Cn vs tU/c

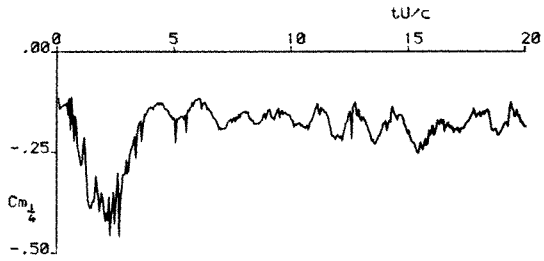

(c) $Cm_{\frac{1}{4}}$ vs tU/c

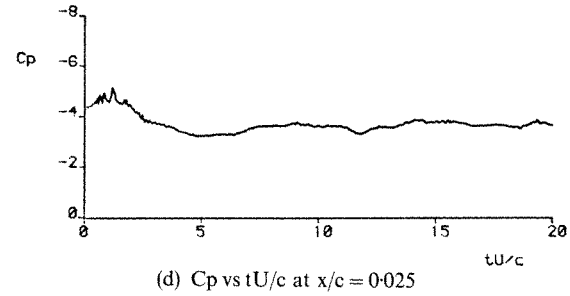

(d) Cp vs tU/c at x/c = 0·025

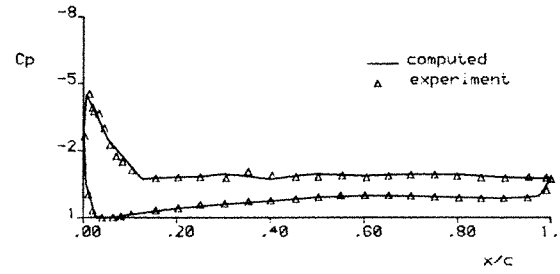

(e) Comparison between computed and steady experimental Cp

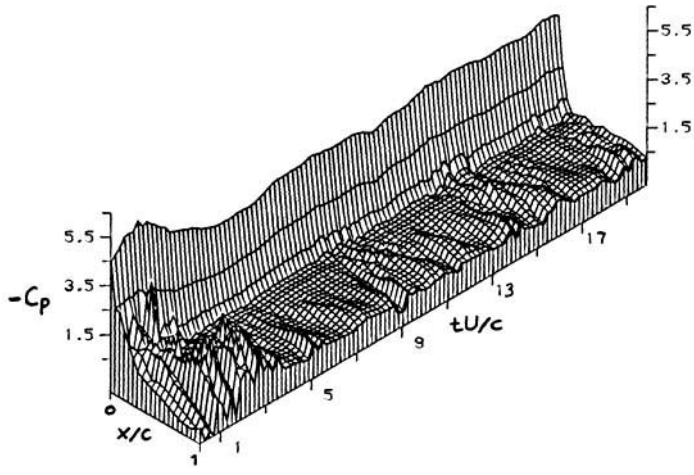

(f) Pressure–time history

Figure 7. Results obtained following a step change in incidence from 0→21·14° using the GA(W)-1 aerofoil

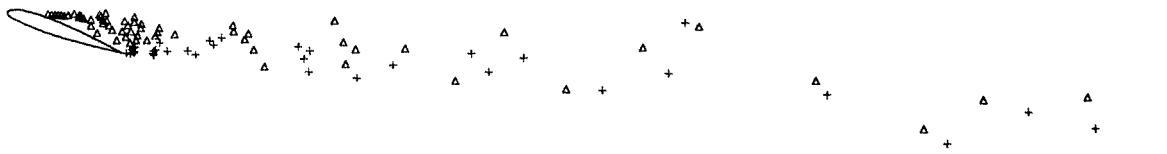

(a) Wake at tU/c = 15
△ clockwise circulation + anticlockwise circulation

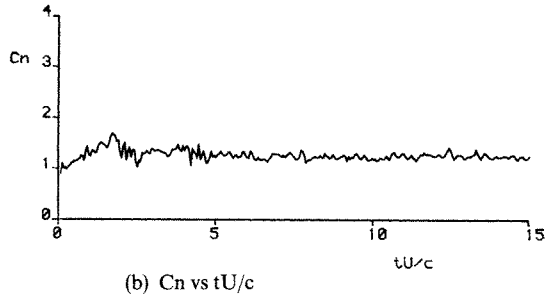

(b) Cn vs tU/c

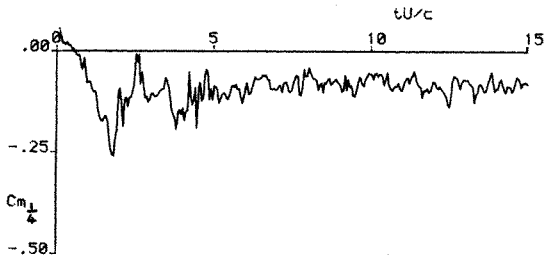

(c) $Cm_{\frac{1}{4}}$ vs tU/c

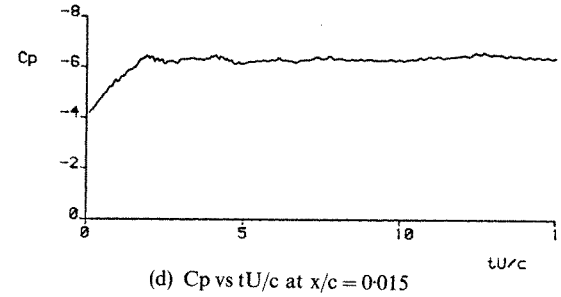

(d) Cp vs tU/c at x/c = 0·015

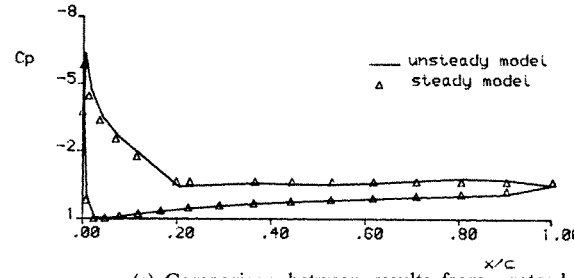

(e) Comparison between results from unsteady and steady model

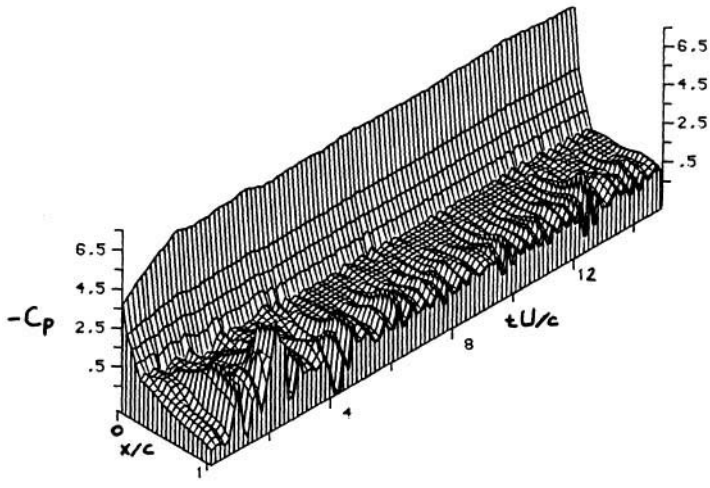

(f) Pressure–time history

Figure 8. Results obtained following a step change in incidence from 0 → 18·60° using the NACA 23012 aerofoil

$tU/c = 20$, that exhibits the closest approximation to a uniform wake pressure. The pressure time history is shown in Figure 7(f), which illustrates well the vortex shedding and subsequent passage over the aerofoil.

The final test case, illustrated in Figure 8, is that of a NACA 23012 aerofoil which undergoes a step change in incidence form 0–18·60°, with $\Delta\theta_p = 0°$ and $x_s/c = 0{\cdot}2$. Because of the lower angle of attack the wake in Figure 8(a) is not as wide as that in Figure 7(a), although the far wake broadens out more in this case than in either of the two cases of separation nearer the trailing edge. The shear layers break up soon after being shed and transform into alternately signed clusters which are convected downstream. The normal force and quarter chord moment can be seen to approach a steady value in Figures 8(b) and 8(c) although the moment exhibits more of the unsteady fluctuations, a feature which can be discerned from all of the results presented herein. The leading-edge pressure in Figure 8(d) builds up to a final value in a fairly short time and the good correlation between the two pressure distributions can be seen from Figure 8(e). For comparison purposes in this case, a 'steady' calculation[21] was performed at the same angle of incidence and separation point position as those used for the 'unsteady' calculation. From the three-dimensional projection in Figure 8(f) it can be seen that after the passing of the initial vortex the wake pressure remains relatively constant close to the separation point but exhibits increasing amounts of unsteadiness nearer to the trailing-edge. This would suggest the presence of vortex clusters close to the aerofoil in this region.

CONCLUSIONS

A new method for the prediction of unsteady, incompressible, separated flow around an arbitrary aerofoil has been developed. An inviscid formulation is used for the flow field and the shear layers are represented by discrete vortices with finite cores. The first results of asymptotically steady separated flow about an aerofoil with a fixed separation point are most encouraging. The algorithm is thus regarded as being very useful and future work will be concerned with the incorporation of a moving separation point into the model to enable a proper investigation of aerofoil dynamic stall during ramp and oscillatory motions to be carried out.

SYMBOL GLOSSARY

A	total influence coefficient of γ_j
C_n	normal lift coefficient
$C_{m\frac{1}{4}}$	quarter chord moment coefficient
C_p	pressure coefficient
c	aerofoil chord
D_0, D_v	distance parameters associated with coalescence
d_1, d_2	distances associated with error estimation
e_v	error estimate of coalescence
G	discrete vortex coefficient
$h, \Delta h$	total head
K	discrete vortex strength
L	aerofoil panel length
N	number of panels
N_v	number of discrete vortices
N_c	number of recently shed vortices not involved in coalescence
$\hat{\mathbf{n}}$	unit normal vector

p	pressure
$\mathbf{q}$	velocity vector
R_1, R_2	regions with different total head
$\mathbf{r}$	position vector
s	distance along panel
$t, \Delta t$	time
$\mathbf{U}$	free-stream velocity
x, y	co-ordinates of points on surface
z	complex number

Greek symbols

Γ	circulation
γ	vorticity strength
Δ, λ	wake panel lengths
η	regulating function associated with vortex core
$\theta, \Delta\theta$	wake panel angles
ρ	density
σ	radius of vortex core
$\phi, \Delta\phi, \phi_c$	velocity potential
ω	vorticity

Subscripts

a, a′, b, b′	positions either side of vortex sheet
i, j	index of aerofoil panels
m	time-step counter
n	normal direction
p	index of wake panels
s	conditions at separation point
v	discrete vortex

REFERENCES

1. M. Vezza, and R. A. McD. Galbraith, 'A method for predicting unsteady potential flow about an aerofoil', *GU Aero Report No. 8401*, February 1984.
2. W. J. McCroskey, 'Unsteady airfoils', *Annual Review of Fluid Mechanics*, **14,** 285–311 (1982).
3. J. P. Geising, 'Non-linear two-dimensional unsteady potential flow with lift', *J. Aircraft*, **5,** (2), 135–143 (1968).
4. B. C. Basu and G. J. Hancock, 'The unsteady motion of a two-dimensional aerofoil in incompressible, inviscid flow', *J. Fluid Mechanics*, **87,** Part 1, 159–178.
5. N. D. Ham, 'Aerodynamic loading on a two-dimensional airfoil during dynamic stall', *A.I.A.A. Journal*, **6,** (10), 1927–1934 (1968).
6. N. Baudu, M. Sagner and J. Souquet, 'Modelisation du dechrochage dynamique d'un profil oscillant', *AAAF 10th Colloque d'Aeronautique Appliquee*, Lille, France, 1973.
7. K. Ono, K. Kuwahara, and K. Oshima, 'Numerical analysis of dynamic stall phenomenon of an oscillating airfoil by the discrete vortex approximation', *Paper No. 8, 7th International Conference of Numerical Methods in Fluid Dynamics*, Stanford, California, 1980.
8. R. R. Clements and D. J. Maull, 'The representation of sheets of vorticity by discrete vortices', *Prog. in Aerospace Sci.*, **16,** (2), 129–146 (1975).
9. T. Sarpkaya, 'An inviscid model of two-dimensional vortex shedding for transient and asymptotically steady separated flow over an inclined plate', *J. Fluid Mech.*, **68,** 109–128 (1975).
10. J. Katz, 'A discrete vortex method for the non-steady separated flow over an airfoil', *J. Fluid Mech.*, **102,** 315–328 (1981).

11. A. Fage and F. C. Johansen, 'On the flow of air behind an inclined flat plate of infinite span', *Proc. Royal Soc. A.*, **116,** 170–197 (1927).
12. W. R. Sears, 'Some recent developments in airfoil theory', *J. of Aero. Sci.*, **23,** (5), 490–499 (1956).
13. W. R. Sears, 'Unsteady motion of airfoils with boundary layer separation'. *A.I.A.A. Journal*, **14,** (2), 216–220 (1976).
14. A. Leonard, 'Vortex methods for flow simulation', *J. Comp. Phys.* **37,** 289–335 (1980).
15. P. R. Spalart, A. Leonard and D. Baganoff, 'Numerical simulation of separated flows', *NASA T.M. 84328*, February 1983.
16. L. M. Milne-Thomson, '*Theoretical Hydrodynamics*, MacMillan and Co. Ltd., London, 2nd Edition, p. 77.
17. L. M. Milne-Thomson, '*Theoretical Aerodynamics*, Dover Publications Inc., New York, 4th Edition, pp. 168–169.
18. M. Vezza and R. A. McD. Galbraith, 'Modelling of unsteady, incompressible, separation on an aerofoil using an inviscid flow algorithm', *GU Aero. Report No. 8412*, November 1984.
19. J. P. Geising, 'Vorticity and the Kutta condition for unsteady multienergy flows', *Trans. A.S.M.E., J. Appl. Mech.*, **91,** 608–613 (1969).
20. B. Maskew and F. A. Dvorak, 'The prediction of Clmax using a separated flow model', *J. A.H.S.*, **23,** (2), 2–8 (1977).
21. J. G. Leishman, J. Hanna and R. A. McD. Galbraith, 'Modelling of trailing-edge separation on arbitrary two-dimensional aerofoils in incompressible flow using an inviscid flow algorithm', *G.U. Aero Report No. 8202*, May 1982.
22. R. J. McGhee and W. D. Beasley, 'Low speed aerodynamic characteristics of a 17-percent-thick aerofoil section designed for general aviation applications', *NASA TN D-7428*, 1973.